

# Fast Linearized Coronagraph Optimizer (FALCO) II: Optical Model Validation and Time Savings over Other Methods

Erkin Sidick\*, A J Eldorado Riggs, Garreth Ruane, John Krist, Dwight Moody, Carl Coker  
Jet Propulsion Laboratory, California Institute of Technology, 4800 Oak Grove Drive, Pasadena, CA 91109

## ABSTRACT

We have developed the Fast Linearized Coronagraph Optimizer (FALCO), a new software toolbox for high-contrast, coronagraphic wavefront sensing and control. FALCO rapidly calculates the linearized deformable mirror (DM) response matrices, also called control Jacobians, and can be used for the design, simulation, or testbed operation of several types of coronagraphs. In this paper, we demonstrate that the optical propagation used in FALCO is accurate and matches PROPER. In addition, we demonstrate the drastic reduction in runtime when using FALCO for DM Jacobian calculations instead of the conventional method used, for example with a model of the Wide-Field Infrared Survey Telescope (WFIRST) Coronagraph Instrument (CGI). We then compare the relative accuracy between optical models in FALCO and PROPER.

**Keywords:** Coronagraphy, adaptive optics, deformable mirrors, space telescopes, exoplanets

## 1. INTRODUCTION

Fast Linearized Coronagraph Optimizer (FALCO) is a new software library used for high-contrast, coronagraphic wavefront sensing and control. It rapidly calculates linearized deformable-mirror (DM) response matrices or control Jacobians and can be used for the design, simulation, or testbed operation of several types of coronagraphs. It is described in detail in this volume by Riggs. *et al.* [1]. In this paper, we demonstrate that the optical propagation used in FALCO is accurate and agrees well with PROPER in appropriate cases. We show the reduction in computation time when using FALCO for DM Jacobian calculations relative to the conventional method used, for example, with the Phase A model of the Wide-field Infrared Survey Telescope (WFIRST) Coronagraph Instrument (CGI). We do so by optimizing a 2-D Hybrid Lyot Coronagraph (HLC) from scratch. We also show the relative accuracy of the control Jacobians calculated by using FALCO and PROPER.

This paper has two more companions in this volume. In one of them Coker *et al.* describe the optimization of key coronagraph design parameters [2]. In the other G. Ruane and others present their results on coronagraph design survey for obstructed and segmented apertures obtained with FALCO [3].

## 2. BACKGROUND

### 2.1 The HLC Optical System

We will optimize an HLC design similar to Phase A model of WFIRST CGI with FALCO and compare its broadband contrast performance with that obtained with PROPER in this paper. We also compare the speed of FALCO versus PROPER by calculating the control Jacobians in those two software tools. For that end, we provide some background information on HLC optical model and Electric-Field Conjugation (EFC) wavefront control (WFC) algorithm in this section.

The key elements of an HLC layout in the  $xz$ -plane is shown in Figure 1. The starlight is delivered to the HLC input pupil (Pupil-1) by a telescope. On the Occulting Mask Coronagraph (OMC) testbed at JPL, we use a supercontinuum, broadband light source centered at wavelength  $\lambda_c=550\text{nm}$  or  $\lambda_c=575\text{nm}$  in combination with five 2%-bandpass filters. In the simulations of this paper, we assume the input broadband light consists of 5 monochromatic light beams whose wavelengths are equal to 546.25, 560.625, 575, 589.375 and 603.75nm. A pair of 48x48-actuator Xinetics deformable mirrors, DM1 and DM2, is placed in series in a shared collimated beam and forms the WFC subsystem. DM1 is conjugate

---

\*Erkin.Sidick@jpl.nasa.gov; Phone 1 818 393-7585; Fax 1 818 393-3290; [www.jpl.nasa.gov](http://www.jpl.nasa.gov)

to the input pupil, and DM2 is one meters downstream. The two DMs provide the control of both phase and amplitude errors from the telescope. The coronagraphic subsystem is made of just two elements, a focal-plane mask (FPM) and a Lyot stop. The lenses in the diagram represent the powered elements in the system.

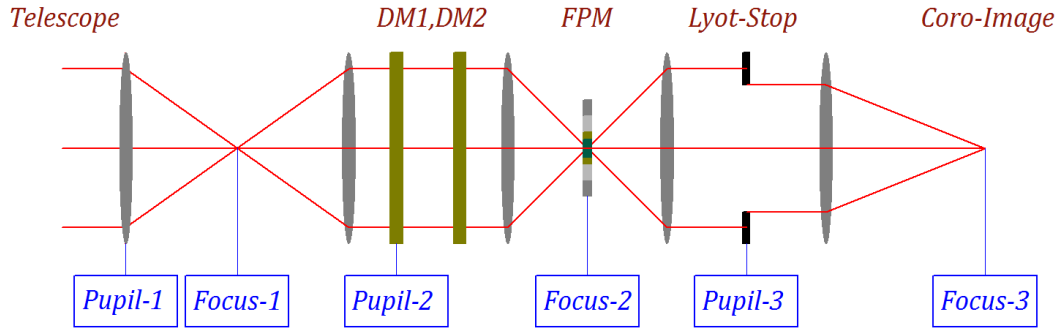


Figure 1. The key elements of the Hybrid Lyot Coronagraph (HLC) testbed layout. The light source (to simulate starlight) is a collimated beam delivered by a telescope to input pupil (Pupil-1), and a sCMOS science camera is located at the coronagraphic image (Coro-Image, Focus-3) plane for detecting the image of the “starlight”.

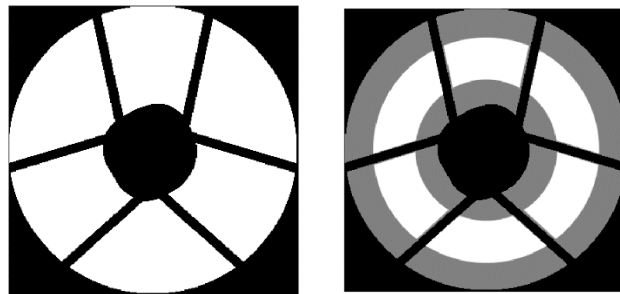


Figure 2. (a) The telescope obscuration pattern shown as an input pupil amplitude. (b) The Lyot-Stop. The pupil, as projected to the coronagraph, is shown in black, the Lyot stop in gray and black, and the pattern of the transmitted light is in white. Both the pupil and the Lyot stop are similar in shape to those used on the OMC testbed.

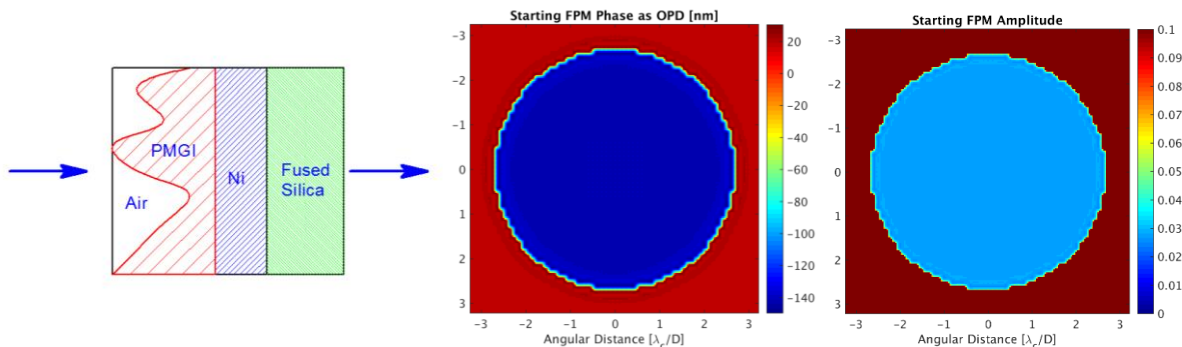


Figure 3. (Left) Thin-film structure of the Focal Plane Mask (FPM). It consists of four layers: Air, dielectric (PMGI), metal (Ni) and a glass substrate (fused silica). (Middle) FPM phase shown as an optical path difference (OPD) in nm. It is obtained with the starting PMGI thickness of 169nm and a Ni thickness of 70nm at the center wavelength of  $\lambda_c = 575\text{nm}$ . (Right) The corresponding FPM amplitude.

The WFIRST telescope pupil, as shown in Fig. 2(a), is obscured by the secondary mirror and its six support struts. The DMs are used in combination with a focal plane occulting mask and a Lyot plane mask, as shown in Fig. 2(b), to generate the high-contrast dark hole. The DMs are also used to correct for static optical design and manufacturing imperfections and to compensate for slow thermal drift in the telescope optics. In Fig. 2(b), the pupil, as projected to the coronagraph, is shown in black and the Lyot stop in gray and black.

The occulting mask used in both the OMC testbed and our simulations are fabricated by depositing a reflective metal disk on a glass substrate first, then depositing a shaped, transparent dielectric layer on top of the metal. That is, it consists of a four-layer thin-film structure as shown in Fig. 3(left). An atomic force microscope scan of a typical occulting mask is provided on Fig. 10 of Ref. [4]. In this paper we use a PMGI thickness of 169nm and a Ni thickness of 70nm as the starting parameters. These thicknesses result in an FPM having a phase and an amplitude maps shown in Figs. 3(middle, right), respectively.

## 2.2 Definitions of Normalized Intensity and Contrast

For the current optical system with two DMs, we carry out wavefront control over an annular (360-deg) dark-hole region bound by  $R_{\min} = 2.7\lambda_c/D$  and  $R_{\max} = 9\lambda_c/D$ ,  $D \sim 48\text{mm}$  is the diameter of the input pupil aperture,  $R = \sqrt{x^2 + y^2} / f$ , and  $f$  is the system focal-length. In this paper we evaluate the contrast performance of the HLC using a normalized intensity. It is defined as

$$I(x, y) = I_o(x, y) / I_{uo\max}, \quad (1)$$

where  $I_o(x, y)$  is the image intensity of the occulted star, and  $I_{uo\max}$  is the peak value of the un-occulted star intensity. It is closely related to the contrast, the metric used most commonly in the fields of high-contrast imaging. The contrast of a field is defined as the planet-to-star flux ratio when the peak pixel of the planet's point spread function (PSF) is equal to the mean per-pixel brightness of the field [5]. We will keep track the value of one metric in this paper, the mean broadband normalized intensity (NI), or  $I_{bb}$ . The  $I_{bb}$  is the mean value of a broadband normalized intensity map inside an annular region from  $2.7\lambda_c/D$  to  $9\lambda_c/D$ . The broadband image intensity is obtained by simply averaging the narrowband or the monochromatic light intensities at 5 different wavelengths.

## 2.3 WFC Algorithm and $\beta$ -Value

In this paper, we use a control algorithm similar to the “minimum-wavefront and optimal control compensator” described in detail in Ref. [6]. This approach is also called “actuator regularization” and “Electric Field Conjugation, EFC” [7]. The WFC algorithm described in Ref. [6] uses the wavefront phase at the system exit pupil as its input, and calculates the actuator commands as its output. In the present case of EFC, we set the DM actuators to superpose the negative of the E-field onto the image plane, with a goal to make the image intensity zero on the dark-hole region on the image plane. Therefore, the WFC algorithm uses an E-field column-vector  $\vec{\mathbf{e}}$  as its input, where

$$\vec{\mathbf{e}} = \begin{bmatrix} \Re(\vec{\mathbf{E}}) \\ \Im(\vec{\mathbf{E}}) \end{bmatrix}. \quad (2)$$

The joint cost function now becomes as

$$J = \frac{1}{2} (\vec{\mathbf{e}}^T \vec{\mathbf{e}} + C_{wu} \vec{\mathbf{u}}^T \vec{\mathbf{u}}), \quad (3)$$

and the gain matrix  $\tilde{\mathbf{G}}$  or G-matrix is obtained from

$$\tilde{\mathbf{G}} = [\tilde{\mathbf{S}}^T \tilde{\mathbf{S}} + C_{wu} \tilde{\mathbf{I}}]^{-1} \tilde{\mathbf{S}}^T. \quad (4)$$

In Eq. (2),  $\vec{\mathbf{E}}$  is the column-vector of the complex E-field on the dark-hole region, and in Eq. (3) the  $C_{wu}$  is the actuator regularization coefficient.  $\vec{\mathbf{E}}$  is formed by stacking the elements of the complex E-field inside the dark-hole region in a certain order, as was explained in Eq. (1) of Ref. [6]. The  $\Re(\vec{\mathbf{E}})$  and the  $\Im(\vec{\mathbf{E}})$  are the real and the imaginary parts of  $\vec{\mathbf{E}}$ , respectively. In Eq. (4), the  $\tilde{\mathbf{S}}$  is the sensitivity matrix consisting of the influence functions of all actuators. It is also called “DM actuator response matrix” [5] and “control Jacobian” [8]. In Eq. (3),  $\vec{\mathbf{u}}$  is a column-vector of the actuator commands.

When operating the HLC testbed, the operator of the testbed does not have direct access to the complex E-field in the coronagraphic image-plane. Therefore, the operator does a wavefront estimation with a pairwise estimation scheme, in which “probes” are placed on one DM to modulate the electric field across the region of interest [8, 9]. Given two or more pairs of probes, along with an image with no probes at all, both the complex E-field of the residual simulated starlight and the portion of the Efielddfsdfs-field that does not interact with the probes and hence is unlikely to be correctable can be estimated (The components that do and do not interact with the probes are referred to as the “coherent” and “incoherent” parts, or “modulated” and “unmodulated” components, respectively). More details of the EFC algorithm and its testbed implementation are given in Refs. [7, 8].

Instead of  $C_{wu}$ , our testbed team at JPL prefers to use a different regularization coefficient called “ $\beta$ -value”. The two coefficients are related by

$$\begin{aligned} \tilde{\mathbf{G}} &= [\tilde{\mathbf{S}}^T \tilde{\mathbf{S}} + C_{wu} \tilde{\mathbf{I}}]^{-1} \tilde{\mathbf{S}}^T = [\tilde{\mathbf{S}}^T \tilde{\mathbf{S}} + \alpha^2 (10^\beta) \tilde{\mathbf{I}}]^{-1} \tilde{\mathbf{S}}^T \\ \rho &= \text{diag}\{\tilde{\mathbf{S}}^T \tilde{\mathbf{S}}\} \\ \alpha^2 &= \max\{\rho\} \end{aligned} \quad (5)$$

where “diag” means “diagonal elements”, and “max” means “maximum value”. One of the advantages of this new choice is that the optimum values of  $\beta$  corresponding to different coronagraph configurations, such as HLC and SPC, become comparable. That is, the value of  $\alpha$  is different for different optical control systems, but the  $\beta$  has the same interpretation for different systems and different control iterations. In Eqn. (5), the  $\rho$ -value is an indicator of relative actuator strength. In the coronagraph studies we got involved with, the value of  $C_{wu}$  is usually positive, but the value of  $\beta$  is usually negative.

The simulation results to be presented in this paper exclude the errors associated with the complex E-field estimation process by obtaining the complex E-field at the final focal plane directly. The simulation creates a 972x972-pixel E-field at the final image plane for an aperture of 324 pixels across, with 3 pixels per  $f\lambda/D$ . Considering only the pixels in the dark-hole and 5 wavelengths gives an E-field vector,  $\vec{\mathbf{e}}$ , having 20,760 field pixels at  $0.33\lambda/D$  sampling. There are a total of  $48 \times 48 \times 2 = 4608$  DM actuators in the current 2-DM system, but we use only the central 3,418 actuators for EFC. So  $\tilde{\mathbf{S}}$  of DM1 and DM2 has a size of 20,760 x 3,418 elements.

### 3. HLC OPTIMIZATION EXAMPLE

#### 3.1 FALCO Autonomous Optimization (Step 1)

We have developed a 2-step optimization approach for FALCO. In the first step, we optimize the surface heights of the DM1 and DM2 in an autonomous way. That is, we update the Jacobians at each control iteration, and for each set of Jacobians we scan the  $\beta$ -value with five values,  $\beta = [-1, -2, -3, -4, -5]$ . At the end of each scan, the program selects the  $\beta$ -value that yields the largest improvement in average dark-hole contrast.

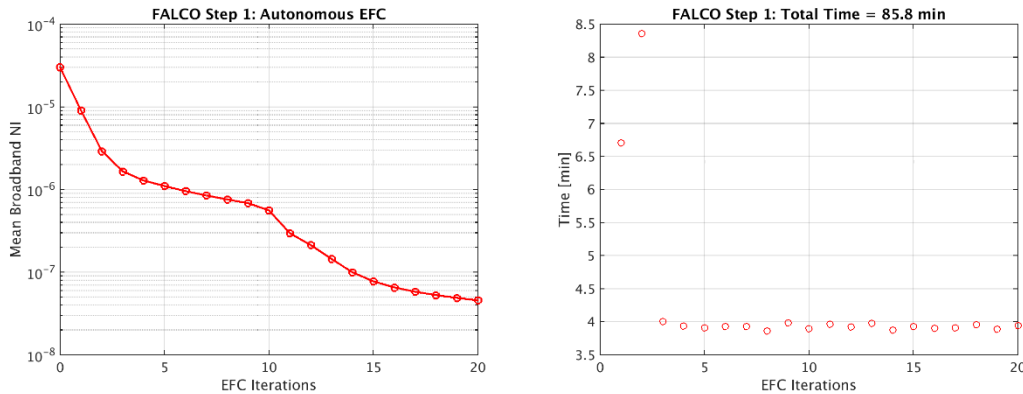


Figure 4. The mean broadband normalized intensity (a) and the runtime (b) versus EFC iteration number in Step 1. At each EFC iteration, FALCO rapidly calculates the five-wavelength DM1 and DM2 Jacobians and then carries out EFC six times for six different  $\beta$ -values. The set-up time is dominated by computing look-up tables, which are then stored to save time in future trials.

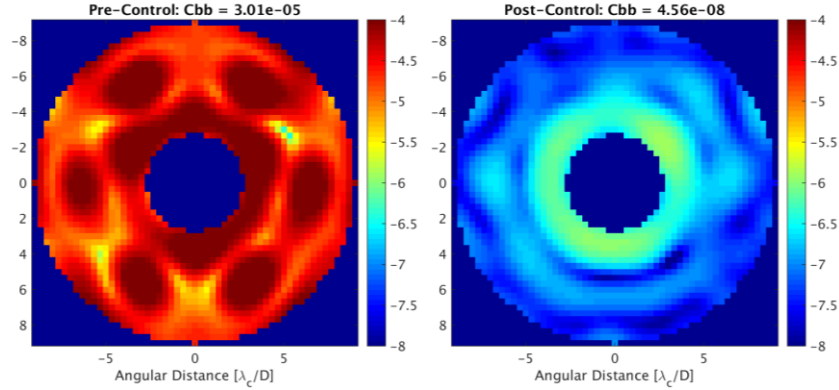


Figure 5. (a) Broadband normalized intensity map,  $I(x, y)$ , corresponding to  $I_{tr} = 0$  in Fig. 4(a), where “ $I_{tr}$ ” means “Iteration”. (b) The  $I(x, y)$  corresponding to  $I_{tr} = 20$  (end data point) in Fig. 4(a).

Figure 4(a) shows the broadband contrast,  $I_{bb}$ , as a function of control iteration, and Fig. 4(b) shows the corresponding time cost. Note that each control iteration includes the calculation of new set of DM1/DM2 Jacobians and six EFC runs with each corresponding to a new  $\beta$ -value. As we can see from part (b), each of such EFC iterations takes only about 4 minutes. In this step, after a total of 20 control iterations, the mean broadband normalized intensity goes down from  $I_{bb} = 3.02E-5$  to  $I_{bb} = 4.56E-8$ . The total time spent during this step is 85.8 minutes.

### 3.2 FALCO “Manual” Optimization (Step 2)

It has been our experience that the autonomous  $\beta$ -scan approach for EFC (such as that used in Step 1) cannot reach nearly as good a contrast as a manual approach with a “down-up-down”  $\beta$ -schedule [10]. The reason has been explained in detail in Ref. [10], and we summarize it here. Briefly speaking, the “down- $\beta$ ” (lower, more aggressive  $\beta$ ) mobilizes a group of actuators that can suppress the “hard-modes” to some degree, but the motion of those actuators increases errors in the “easy-modes”, thus degrading the average contrast value most of the time. But the “up- $\beta$ ” (larger, less aggressive  $\beta$ ) that comes next mobilizes a group of actuators that can suppress those introduced “easy-modes” while leaving the hard-modes where they are. As a result, this EFC process yields much better contrast floor as compared to the autonomous  $\beta$ -scan, which instead gets stuck in a worse local minimum.

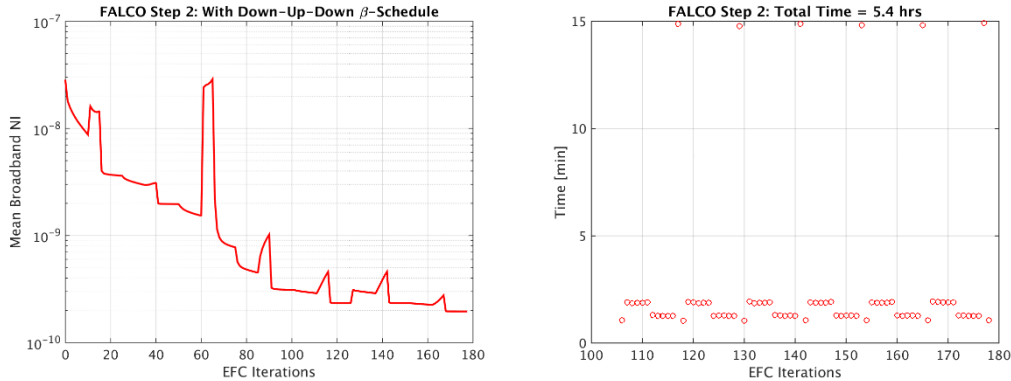


Figure 6. (a)  $I_{bb}$  as a function of EFC iterations. It was obtained with 6 sets of Jacobians, or six sub-steps, with each sub-step having its own Jacobians and “down-up-down”  $\beta$ -schedule. (b) The corresponding time cost. The time peaks correspond to the beginning of sub-steps at which a new set of Jacobians are calculated.

Figures 6(a,b) show the  $I_{bb}$  and the corresponding runtime of FALCO optimization Step 2. In part (a),  $I_{bb}$  is shown as a function of EFC iterations. It was obtained with 6 re-calculations of Jacobians, or six sub-steps, each having its own Jacobians and “down-up-down”  $\beta$ -schedule. The most EFC iterations taken without re-linearizing is 25. Part (b) shows the corresponding time cost. The runtime peaks correspond to the beginning of the sub-steps at which a new set of Jacobians are calculated. Usually it is necessary to adjust the  $\beta$ -values and the corresponding iteration numbers of each sub-steps manually by trial and error to see what values yield the optimum  $I_{bb}$ -value, but in the current case we had to do

this only twice, one for the first 3 Jacobians and the other for the last 3 Jacobians. For example, in the first sub-step we used  $\beta = [-3 \ -4 \ -2]$  and  $N_\beta = [10 \ 5 \ 10]$ , where  $N_\beta$  is the number of control iterations at each  $\beta$ -value.

Figure 7(a) shows the normalized intensity map corresponding to the last data point in Fig. 6(a), and Figs. 7(b,c) show the corresponding DM1 and DM2 actuator heights. The final contrast floor we obtained in this optimization example is  $I_{bb} = 1.96\text{E-}10$ .

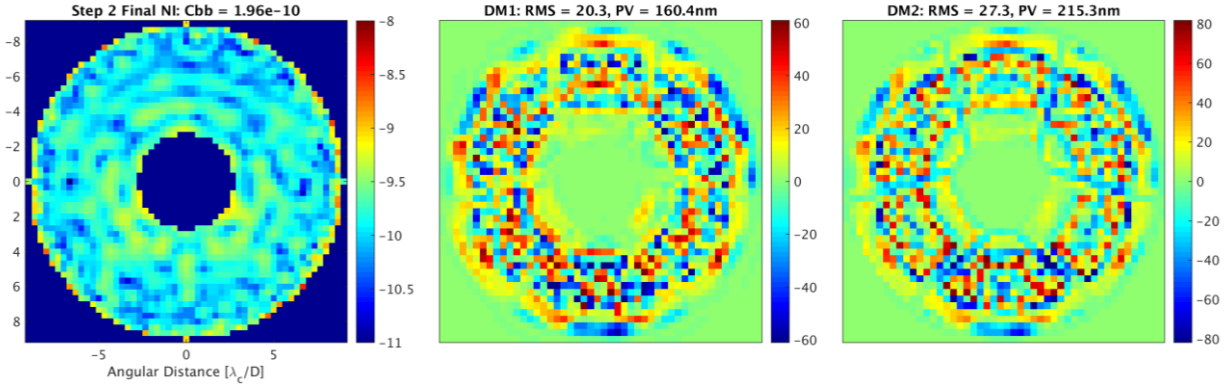


Figure 7. (a) The normalized intensity map corresponding to the last data point in Fig. 6(a). (b,c) The corresponding DM1 and DM2 actuator heights.

#### 4. FALCO VERSUS PROPER: ACCURACY

After evaluating the HLC contrast performance of the PROPER model using the DM1 and DM2 commands (as in in Figs. 7(b,c)) and FPM obtained in FALCO, we obtained an intensity map,  $I(x, y)$ , as shown in Fig. 8(a). After carrying out some additional EFC with two sets of Jacobians (that is, calculating a set of Jacobians at the beginning and updating them once), we obtained an improved contrast floor as shown in Fig. 8(b) as well as in Figs. 9(a-c).

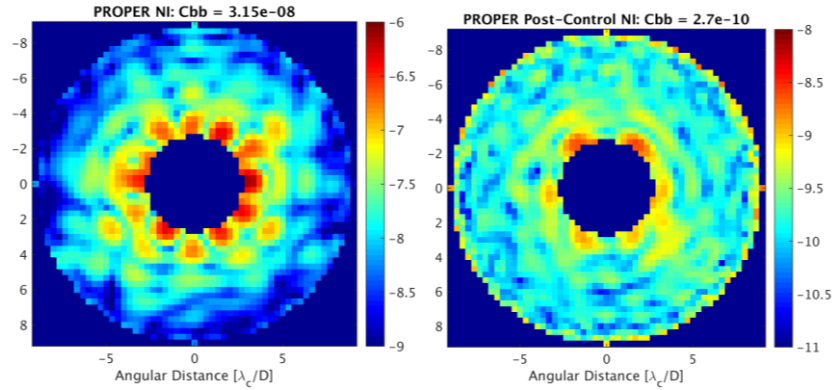


Figure 8. (a)  $I(x,y)$  map obtained using the DM1, DM2 and DM3 actuator solutions obtained in FALCO, the ones corresponding to the last data point in Fig. 6(a). (b)  $I(x,y)$  map obtained after carrying out two sub-steps of additional EFC in PROPER.

One of the differences between FALCO and PROPER is that FALCO uses physical length unit on all optical surfaces, but PROPER uses “pixels” as the unit of length on all optical surfaces. This is because PROPER uses only fast Fourier transforms (FFTs), whereas FALCO uses matrix Fourier transforms (MFTs) to maintain the same plate scale at the image for all wavelengths. This introduces differences at the final image-plane when the wavelength is not equal to the center-wavelength. That is because in PROPER we adjust the zero-padding of the final pupil-plane (Lyot-plane) E-field such that the samplings of the final image plane E-fields with different wavelengths match with one another, but in general the

number of points across the array has to be rounded, which introduces errors. One could instead use the `prop_magnify` function PROPER to re-scale the plate scale, which would add more time to the computation.

Figure 10 compares the real and the imaginary parts of the final image-plane E-field at  $\lambda = \lambda_c$  obtained with FALCO and PROPER, respectively, and their differences. The differences in E-fields between FALCO and PROPER is negligible and is near the numerical noise floor.

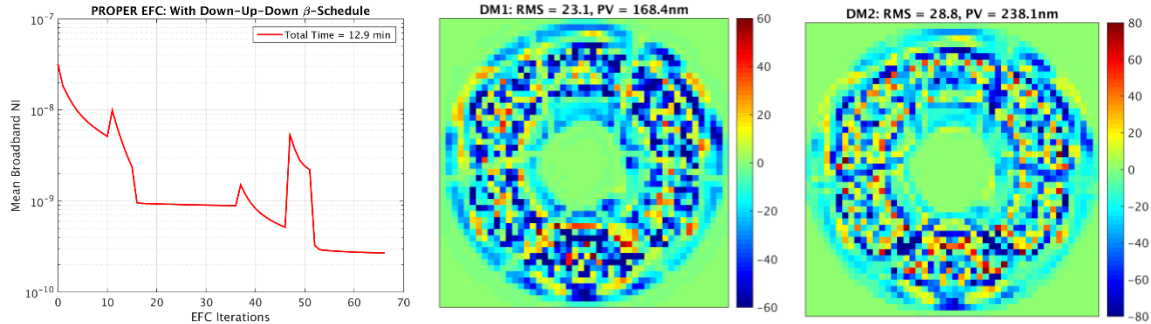


Figure 9. (a)  $I_{bb}$  as a function of EFC iterations obtained with PROPER. It was obtained with 2 sets of Jacobians, or two sub-steps, each sub-step having its own Jacobians and ‘down-up-down’  $\beta$ -schedule. (b,c) DM1 and DM2 actuator heights corresponding to the last data point in part (a).

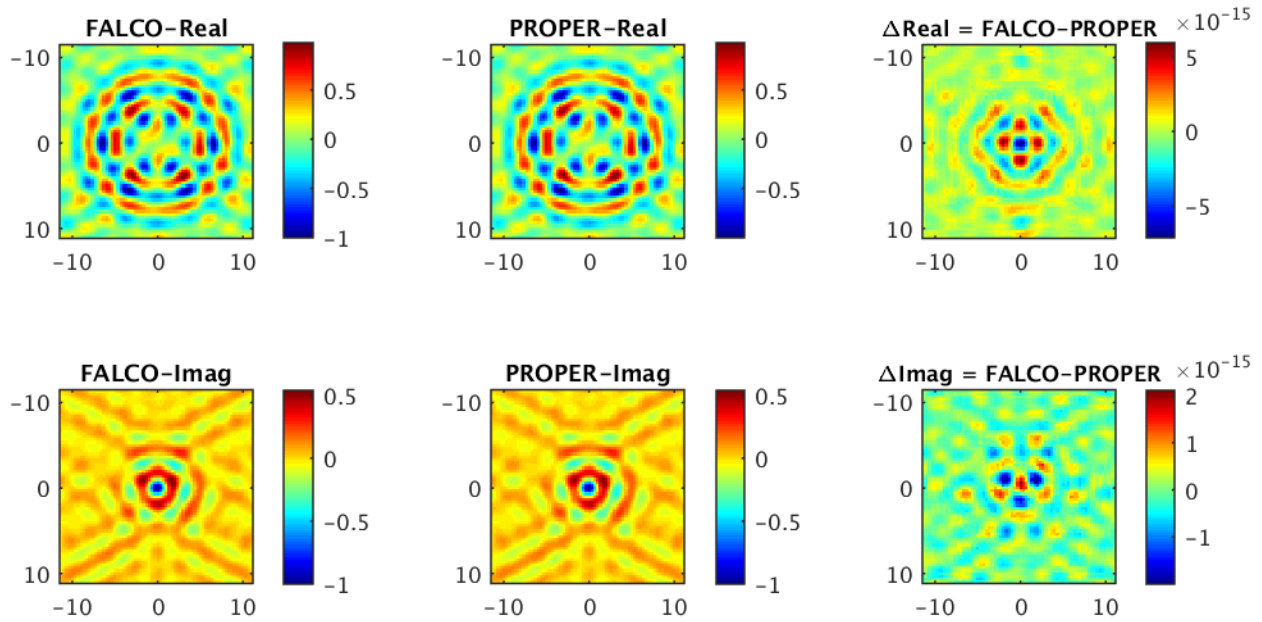


Figure 10. The real and the imaginary parts of the final image-plane E-fields at the center wavelength of 575nm. The field maps on the first column were obtained with FALCO, the second with PROPER and the third are their differences. ‘Real’ and ‘Imag’ mean the real and the imaginary components of the E-field, respectively.

## 5. FALCO VERSUS PROPER: RUNTIME

The Jacobian computation times in FALCO and PROPER are compared in Table 1 for optimization Step 1 and Step 2, separately. We did not carry out Step 1 optimization with PROPER, and used the computation times of Step 2 for this comparison. When calculating Jacobians, FALCO uses a linearized model which runs much faster relative to the conventional approach used in PROPER. As a result, calculating the DM1 and DM2 Jacobians with FALCO is 61 times faster than with recovered the better speed from Step 1 with recent updates to FALCO.

Some of the results in Table 1 are shown graphically with a bar-plot in Fig. 11. Note that “DM3” is actually the FPM, which we give its own basis set for optimizing its profile.

Table 1: Comparison of Jacobian calculation times needed in FALCO and PROPER.

	Step 1	Step 2			
	DM1+DM2	DM1	DM2	DM3	Total
Number of Active Actuators	3418	1998	1420	2916	6334
PROPER Time [mins]	239.86	140.2	99.66	241.30	481.16
FALCO Time [mins]	3.93	8.72	8.96	21.07	38.75
Time Ratio: PROPER/FALCO	61.03	16.08	11.12	11.45	12.42

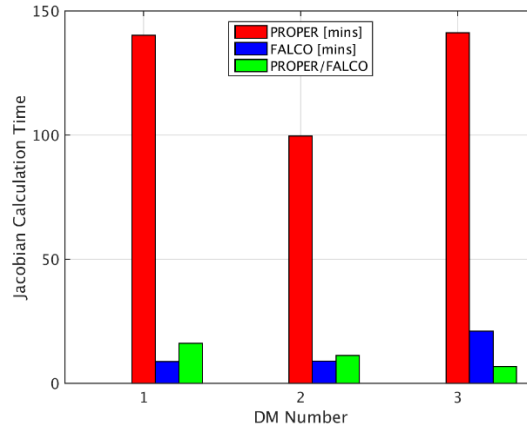


Figure 11. Jacobian calculation times needed in the optimization Step 2 in FALCO and PROPER, respectively, and their ratios.

## 6. CONCLUSION

FALCO is an open-source, modular software collection used for coronagraphy as well as wavefront sensing and control. In this paper, we compared the computation speed and the accuracy of FALCO with PROPER. By optimizing a Hybrid Lyot Coronagraph design from scratch in two steps, we have shown that the time needed to calculate DM response matrix or control Jacobian in FALCO is more than 60 times faster than PROPER when FALCO uses sub-array propagation as appropriate, and it is more than 12 times faster when it uses the conventional method of differencing of E-fields. Such a faster speed in FALCO is also achieved with the help of matrix Fourier transforms (MFTs). We have shown in this paper that FALCO has the same numerical accuracy as PROPER and is tens of times faster than the conventional method of computing control Jacobians.

## 7. ACKNOWLEDGMENTS

The research was carried out at the Jet Propulsion Laboratory, California Institute of Technology, under a contract with the National Aeronautics and Space Administration. The decision to implement the WFIRST mission will not be finalized until NASA’s completion of the National Environmental Policy Act (NEPA) process. This document is being made available for information purposes only.

## REFERENCES

- [1] A.J. Eldorado Riggs\*, Garreth Ruane†, Erkin Sidick\*, Carl Coker\*, Brian Kern, "Fast Linearized Coronagraph Optimizer (FALCO)", Proc. SPIE 10698, (2018).
- [2] Carl T. Coker, A.J. Eldorado Riggs, Erkin Sidick, Byoung-Joon Seo, Brian D. Kern, David S. Marx, Stuart B. Shaklan, "Fast linearized coronagraph optimizer (FALCO) III: Optimization of key coronagraph design parameters", Proc. SPIE 10698, (2018).
- [3] Garreth Ruane<sup>1</sup>, A J Eldorado Riggs, Carl Coker, Stuart Shaklan, Erkin Sidick, Jeffrey Jewell, Dimitri Mawet<sup>1</sup>, Kunjithapatham Balasubramanian, Chris Stark, "Fast Linearized Coronagraph Optimizer (FALCO) IV. Coronagraph design survey for obstructed and segmented apertures", Proc. SPIE 10698, (2018).
- [4] F. Shi, *et al*, "Low order wavefront sensing and control for WFIRST Coronagraph," Proc. SPIE, vol. 9904, pp. 990418, August 2016.
- [5] John Krist, Bijan Nemati, and Bertrand Mennesson, "Numerical modeling of the proposed WFIRST-AFTA coronagraphs and their predicted performances," J. Astron. Telesc. Instrum. Syst. 2(1):011003 (2016).
- [6] Erkin Sidick, Scott A. Basinger, and David C. Redding, "An improved wavefront control algorithm for large space telescopes," Proc. SPIE, **7015**, 70154P (2008).
- [7] Amir Give'on *et al*, "Broadband wavefront correction algorithm for high-contrast imaging system," Proc. SPIE, **6691**, 66910A (2007).
- [8] Eric Cady, *et al*, "Demonstration of high contrast with an obscured aperture with the WFIRST-AFTA shaped pupil coronagraph," J. Astron. Telesc. Instrum. Syst. 2(1):011004 (2015).
- [9] A. Give'on, B. D. Kern, and S. Shaklan, "Pair-wise, deformable mirror, image plane-based diversity electric field estimation for high contrast coronagraphy," Proc. SPIE 8151, 815110 (2011).
- [10] Erkin Sidick, Byoung-Joon Seo, Brian Kern, David Marx, Ilya Poberezhskiy, and Bijan Nemati, "Optimizing the Regularization in Broadband Wavefront Control Algorithm for WFIRST Coronagraph," Proc. SPIE, vol. 10400, vol. pp.1040022-1, August 2017.